

## Investigation of Neutron-Irradiated Microstructure of Fe-Cr System: A GPU Accelerated Phase-field method

Jeonghwan Lee, Kunok Chang\*

<sup>a</sup>Nuclear Engineering, Kyung Hee Univ., Republic of Korea

\*Corresponding author: kunok.chang@khu.ac.kr

### 1. Introduction

Ferritic martensitic steels are promising due to their low swelling rate under the fast neutron irradiation. However, in the case of Fe-Cr steels, precipitation of Cr rich phase ( $\alpha'$  phase) near 475°C is still pointed out as a weak point in the view point of structural integrity. [1][2] therefore, understanding the spinodal decomposition behavior of the Fe-Cr system under the fast neutron irradiation is important topic in studying the integrity of structural materials.

Herein, we analyze the spinodal decomposition behavior under the fast neutron irradiation of the Fe-Cr system using a graphics processing unit(GPU)-accelerated phase-field method. Since high energy particles produce a point defect, we quantify the microstructure evolution behavior of the Fe-Cr system under the fast neutron irradiation.

In addition, we consider the different computational technique. Since the quantitative prediction of the real material system is highly computationally expensive, we have implement a parallel computing scheme based on the compute unified device architecture (CUDA) to improve computational efficiency [3], comparing it with parallelized code using CUDA when solving the Cahn-Hilliard diffusion equation [4] using a semi-implicit spectral method [5].

Although CUDA has previously been applied to the phase-field method, it was used to create an explicit solver [6], [7]. Herein, we instead use it to implement a semi-implicit spectral method and compare the performance of OpenMP- and CUDA-accelerated code. Results will help to guide any researchers aiming to solve the Cahn-Hilliard equation using fast Fourier transform.

### 2. CALPHAD-based phase-field methods

#### 2.1 Semi-implicit Fourier spectral method

We simulate the evolution of the Cr concentration field by solving the following Cahn-Hilliard equation [8]:

$$\frac{\partial c(r,t)}{\partial t} = V_m^2 \nabla \cdot [M(r,t) \cdot \nabla \left( \frac{\delta F(r,t)}{\delta c} \right)] \quad (1)$$

$$F(r,t) = \int_V \left\{ \frac{1}{V_m} [f(c) + \frac{1}{2} \kappa (\nabla c)^2] \right\} dV \quad (2)$$

where  $c$  is the Cr concentration,  $\kappa$  is the gradient energy coefficient,  $F(r,t)$  and  $f(c)$  are the system's molar free energy and molar chemical free energy, respectively.  $f(c)$  is discussed in the following section.

The molar free energy  $F(r,t)$  in Eq.(1) is given by Eq. (2), The gradient coefficient  $\kappa$  is given by

$$\kappa = \frac{1}{6} r_0^2 L_{FeCr} \quad (4)$$

where  $r_0$  is the lattice parameter and  $L_{FeCr}$  is the regular solution interaction parameter.

The mobility  $M$  in the Cahn-Hilliard-Cook equation is assumed to be independent of the concentration field Therefore, rearranged Eq. (1) as

$$\frac{\partial c(r,t)}{\partial t} = \nabla^2 \left[ \left( \frac{\delta f(c)}{\delta c} \right) - \kappa \nabla^2 c(r,t) \right] \quad (5)$$

$$\frac{\partial \tilde{c}(k,t)}{\partial t} = -k^2 \left( \frac{\delta F(r,t)}{\delta c} \right)_k - \kappa k^4 \tilde{c}(k,t) \quad (6)$$

where  $k = (k_1, k_2)$  is the reciprocal vector in the Fourier space of magnitude  $k = \sqrt{k_1^2 + k_2^2}$  and  $\tilde{c}(k,t)$  and  $\left( \frac{\delta F(r,t)}{\delta c} \right)_k$  are the Fourier transforms of  $c(r,t)$  and  $\left( \frac{\delta f(c)}{\delta c} \right)$  respectively. Then, we applied an explicit Euler Fourier spectral treatment to this equation, yielding

$$\frac{\partial \tilde{c}^{n+1}(k,t) - \tilde{c}^n(k,t)}{\Delta t} = -k^2 \left( \frac{\delta F(r,t)}{\delta c} \right)_k^n - \kappa k^4 \tilde{c}(k,t) \quad (7)$$

so

$$\tilde{c}^{n+1}(k,t) = \frac{\tilde{c}^n(k,t) - \Delta t k^2 \left( \frac{\delta F(r,t)}{\delta c} \right)_k^n}{1 + \Delta t \kappa k^4} \quad (8)$$

#### 2.2 Modified CALPHAD-type free energy

The molar chemical free energy  $f(c)$  in Eq. (2) is given by [7, 8]

$$f(c) = (1-c)G_{Fe}^0 + cG_{Cr}^0 + L_{FeCr}c(1-c) + RT[c \ln c + (1-c) \ln(1-c)] + G_m \text{ (J/mol)} \quad (9)$$

where  $G_{Fe}^0$  and  $G_{Cr}^0$  are the molar Gibbs free energies for pure elemental Fe and Cr, respectively,  $L_{FeCr}$  is the interaction parameter between Fe and Cr,  $R (= 8.314) / \text{mol} \cdot \text{K}$  is the gas constant,  $T$  is the system's absolute temperature, which is 563 K herein, and  $G_m$  is the molar Gibbs free energy of the magnetic ordering effect. These were calculated as follows:

$$G_{Fe}^0 = +1225.7 + 124.134 \times T - 23.5143 \times T \times \ln T - 0.00439752 \times T^2 - 5.89269 \times 10^{-8} \times T^3 + 77358.5 \times T^{-1}$$

$$G_{Cr}^0 = -8856.94 + 157.48 \times T - 26.908 \times T \times \ln T \\ + 0.00189435 \times T^2 - 1.47721 \\ \times 10^{-6} \times T^3 + 139250 \times T^{-1}$$

$$L_{FeCr} = +20500 - 9.68T$$

$$G_m = RT \ln(\beta + 1) \lambda(\tau), (\text{J/mol})$$

Where  $\beta$  is the atomic magnetic moment, calculated in terms the Bohr magneton as

$$\beta = 2.22(1 - c) - 0.008c - 0.85c(1 - c).$$

The function  $\lambda(\tau)$  is expressed as the following polynomial:

$$\lambda(\tau) = -0.90530 \tau^{-1} + 1.0 - 0.153\tau^3 - 6.8 \\ \times 10^{-3}\tau^9 - 1.53 \times 10^{-3}\tau^{15} \quad (\tau > 1) \\ = -0.06417 \tau^{-5} - 2.037 \times 10^{-3}\tau^{-15} - 4.278 \\ \times 10^{-4}\tau^{-25} \quad (\tau < 1)$$

Where  $\tau = T/T_c$  is critical magnetic ordering temperature given by

$$T_c = 1043(1 - c) - 311.5c + c(1 - c)[1650 \\ + 550(2c - 1)] (\text{in K})$$

Eq. (2) includes a magnetic ordering contribution to the free energy. Some previous studies have neglected magnetic ordering effects. However, as shown in Fig. 1, the Fe-Cr system's free energy at 563 K varies substantially depending on whether or not magnetic ordering effects are included.

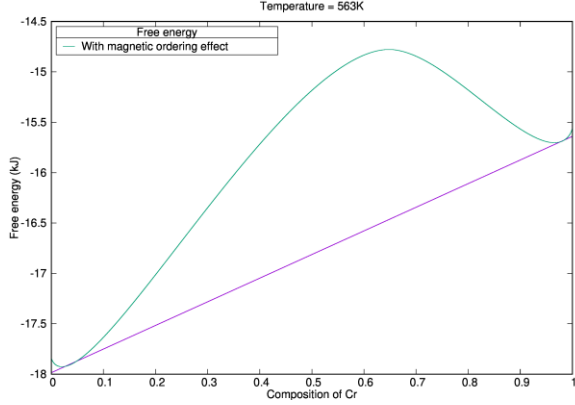


Fig 1: Free energy curve for the Fe-Cr at 563 K with considering magnetic ordering effects. The equilibrium Cr concentration are  $C_{Cr} = 0.05$  and  $C_{Cr} = 0.98$

To increase the computational efficiency, we used dimensionless values herein. Specifically, our simulations used the normalized values  $r^* = r/l$ ,  $\nabla^* = \partial/\partial(r/l)$ ,  $t^* = tD/l^2$ ,  $M^* = V_m RT^* M/D$ ,  $f^*(c) = f(c)/(3RT^*)$ , and  $\kappa^* = \kappa/RT^* l^2$  with  $D = 10^{-24} m^2/s$ ,  $T^* = 900K$ , and  $l = 2.856\text{\AA}$ , where is  $a_0$  value in Eq. (6). We used  $\kappa^* = 2.4901$  when considering magnetic ordering effects [9].

### 2.3 Performance benchmark

To improve the computational efficiency, we apply parallelization technique. In this study, CUDA was used

due to CUDA is most effective when solving the Cahn-Hilliard equation [9]. A semi-implicit Fourier spectral method, as described in the previous section, was implemented by utilizing cuFFT for the CUDA code. For this benchmark, we conducted 2D spinodal decomposition simulations that describe the microstructure evolution behavior of the Fe-Cr system under the fast neutron irradiation. We measured the time taken to calculate 100,000 time steps using the Linux *time* command, which gives the real elapsed time.

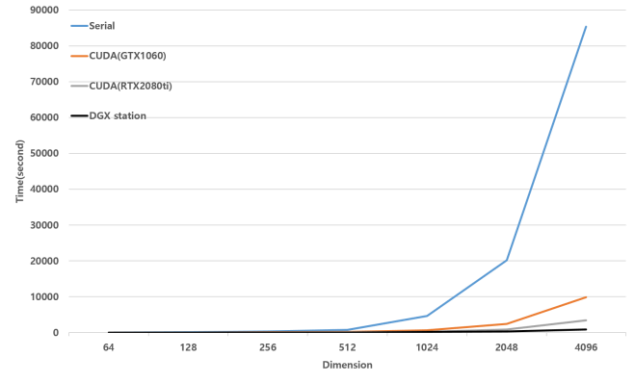


Fig 2: Time consumption for the microstructural evolution simulation with serial (i9-9900K 3.6 GHz CPU) and CUDA (1060, 2080ti and Tesla V100)

We compared the efficiencies of the CUDA-based code on the same or a comparable computer, and the results obtained are shown in Fig. 2. We conducted these comparisons for seven different numbers of dimensions, namely 128, 256, 512, 1024, and 2048. Here, a dimensionality of 128 (say) means that the system cell size was  $128\Delta x \times 128\Delta y$ .

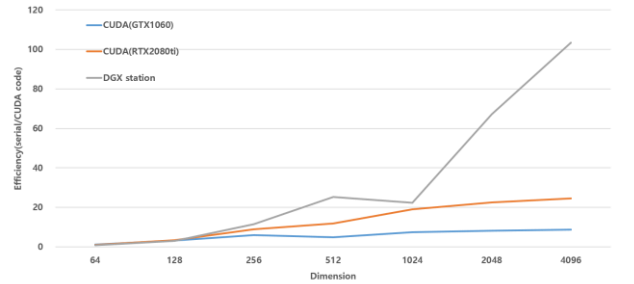


Fig 3: CUDA code efficiency compared to serial code

As shown in Fig. 2 the computational cost of the CUDA code better than serial code. Also, Fig 3, as the system size increases, the efficiency of the CUDA code increases up to 103 times. However, CUDA code is 2% slow when system size is  $64\Delta x \times 64\Delta y$ .

### 2.4 Simulation results and analysis

To investigate the microstructure evolution of the Fe-Cr on phase separation behavior, we performed four sets of simulations shown in Table 1.

Table I: Four sets of simulations for various alloy

	Alloy	Fraction of $\alpha'$ phase	Number of precipitate
Case 1	9Cr	0.060	112
Case 2	12Cr	0.092	221
Case 3	15Cr	0.122	759
Case 4	18Cr	0.154	949

We set a 1000 initial number of precipitate and each case has different initial Cr concentration.

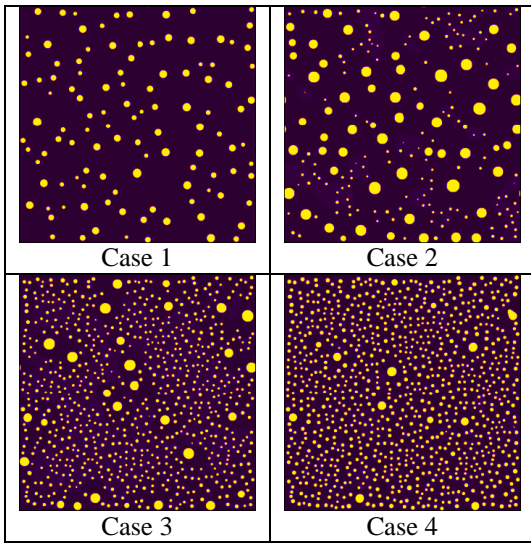


Fig. 5: Plots of the Cr Concentration at  $1.0 \times 10^6$  time step for cases 1-4 in Table 1. The Cr concentration is 1 when yellow area, the black area is 0 Cr concentration

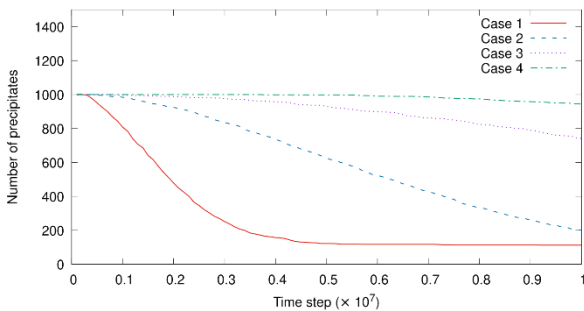


Fig. 6: Plots of the number density of  $\alpha'$  precipitates for cases 1-4 in Table 1

The smaller the initial Cr composition, less the number of precipitates at  $1.0 \times 10^6$  time step. Also, the number of  $\alpha'$  precipitates in case 1 rapidly decrease when early stage.

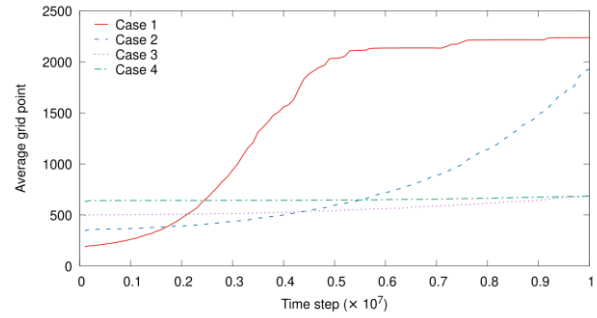


Fig. 7: Plots of the average area of precipitates.

As shown in Fig.7, in the early stages of microstructure evolution in Case 1, the size of precipitates grows rapidly. Also, the smaller the initial Cr composition, the average area of precipitate grows bigger than large Cr concentration.

### 3. Conclusions and future work

Herein, we simulated a set of phase-field models to investigate the phase separation behavior in the Fe-Cr binary alloy system. When the initial composition was between 9Cr and 18Cr, the smaller the initial Cr concentration, the smaller the number of precipitates, and the larger the size of precipitate. So, we analysis microstructure evolution behavior of Fe-Cr system under the fast neutron irradiation.

However, in this study, we did not consider the effect of elasticity. In the future study, we will consider the effect of elasticity on the grain boundary under the fast neutron irradiation.

### REFERENCES

- [1] P. Grobner, The 885 f (475 c) embrittlement of ferritic stainless steels, *Metall. Trans.*, 4(1), pp. 251-260, 1973.
- [2] D. Chandra, L. Schwartz, Mössbauer effect study of the 475 c decomposition of fe-cr, *Metall. Trans.*, 2(2), pp.511-519, 1971.
- [3] C. Nvidia, *Programming guide* 2010.
- [4] J.W. Cahn, J.E. Hilliard, Free energy of a nonuniform system. I. Interfacial free energy, *J. Chem. Phys.*, 28(2), pp. 258-267, 1958
- [5] L.Q. Chen, J. Shen, Applications of semi-implicit fourier-spectral method to phase field equations, *Comput. Phys. Commun.*, 108 (2-3), pp. 147-158, 1998.
- [6] A. Yamanaka, T. Aoki, S. Ogawa, T. Takaki, Gpu-accelerated phase-field simulation of dendritic solidification in a binary alloy, *J. Cryst. Growth*, 318 (1), pp.40-45, 2011.
- [7] J. Hötzer, A. Reiter, H. Hierl, P. Steinmetz, M. Selzer, B. Nestler, The parallel multi-physics phase-field framework pace3d, *J. Comput. Sci.*, 26, pp. 1-12, 2018
- [8] J.W. Cahn, On spinodal decomposition, *Acta Metall.*, 9 (9), pp. 795-801, 1961
- [9] Lee, Jeonghwan, and Kunok Chang. "Effect of magnetic ordering on the spinodal decomposition of the Fe-Cr system: A GPU-accelerated phase-field study." *Computational Materials Science* 169 (2019)